Low-load friction behavior of epitaxial C_{60} monolayers under Hertzian contact

U. D. Schwarz and W. Allers
Institute of Applied Physics and Microstructure Research Center, University of Hamburg, Jungiusstrasse 11, D-20355 Hamburg, Germany

G. Gensterblum
Laboratoire Interdisciplinaire de Spectroscopie Electronique, Facultés Universitaires Notre-Dame de la Paix, 61, rue de Bruxelles, B-5000 Namur, Belgium

R. Wiesendanger
Institute of Applied Physics and Microstructure Research Center, University of Hamburg, Jungiusstrasse 11, D-20355 Hamburg, Germany

(Received 16 May 1995; revised manuscript received 20 July 1995)

Monolayers of C_{60} molecules epitaxially grown on GeS(001) in ultrahigh vacuum were investigated by friction force microscopy in air. The frictional force F_f on the GeS substrate was found to be proportional to the normal force F_n in the first approximation, whereas the friction measured on the first C_{60} monolayer fits excellently to a $F_f \propto F_n^{2/3}$ dependence. This different frictional behavior causes a flip in contrast in spatially resolved friction force maps. Additionally, the second C_{60} monolayer exhibited a lower friction than the first layer at normal forces below the critical force where the contrast flips. The measured data are analyzed using a generalized Hertzian theory, which considers capillary condensation.

I. INTRODUCTION

Although frictional forces play a vital role in daily life and are easily measured, the fundamental mechanisms of friction are poorly understood. The main reason for this is that most macroscopically measurable frictional effects are dominated by the influence of wear, plastic deformation, lubrication, surface roughness, and surface asperities. Pure wearless friction on a molecular scale was experimentally not accessible.

Recently, however, the experimental setups to study tribological systems have been significantly improved. For instance, it has become possible to investigate the sliding of two molecularly smooth surfaces against each other using the surface force apparatus (SFA).[1,2] An even more recent development is the friction force microscope,[3–5] which is derived from the scanning force microscope[6] and enables spatially resolved measurements of lateral forces by moving a sharp tip, representing (approximately) a point contact, over a sample surface.

It is well known that thin layers of some materials can drastically reduce the friction of surfaces ("boundary lubrication").[7] Soon after the discovery of the C_{60} molecule,[8] there have been speculations about possible unique lubricating properties of C_{60} films due to the spherical shape of the individual C_{60} molecules. This spherical shape and the fact that the C_{60} molecules interact only by weak van der Waals interaction allow the C_{60} molecule to rotate freely at room temperature in bulk single crystals[9] as well as in thin films on various types of substrates. However, recent studies of the tribological properties of C_{60} films have led to contradictory conclusions.[10–15]

Here, we report on a nanotribological study of C_{60} films epitaxially grown on layered GeS(001) substrates in ultrahigh vacuum (UHV). Friction force microscopy (FFM) has been applied to probe the local frictional properties of C_{60} thin films with respect to the GeS substrates. The frictional force F_f on the GeS substrate was found to be nearly proportional to the normal force F_n, whereas the frictional behavior of the C_{60} monolayers fits excellently to a $F_f \propto F_n^{2/3}$ dependence. The different loading dependence of the friction on the substrate and the C_{60} monolayers is shown to cause a flip of the contrast in a series of FFM images acquired at different loading forces on the same surface spot. Possible explanations of this behavior in terms of a generalized Hertzian theory are given and will be discussed extensively.

II. EXPERIMENT

GeS is a layered material [Fig. 1(a)] which can be easily cleaved along its (001) plane by using Scotch tape. Its surface structure is rectangular; the lattice constants are $a = 3.64$ Å, $b = 4.30$ Å, and $c = 10.47$ Å.[16] The uncoated crystal exhibits large atomically smooth terraces,[17] similar to, e.g., highly oriented pyrolytic graphite. These terraces are separated from each other by steps of half of the unit-cell height or multiples of this value.

The C_{60} films were sublimated in UHV on *in situ* cleaved single-crystalline GeS(001) substrates of $6 \times 6 \times 0.5$ mm^3 size. The crystallinity of the GeS was checked by means of low-energy electron diffraction (LEED) after

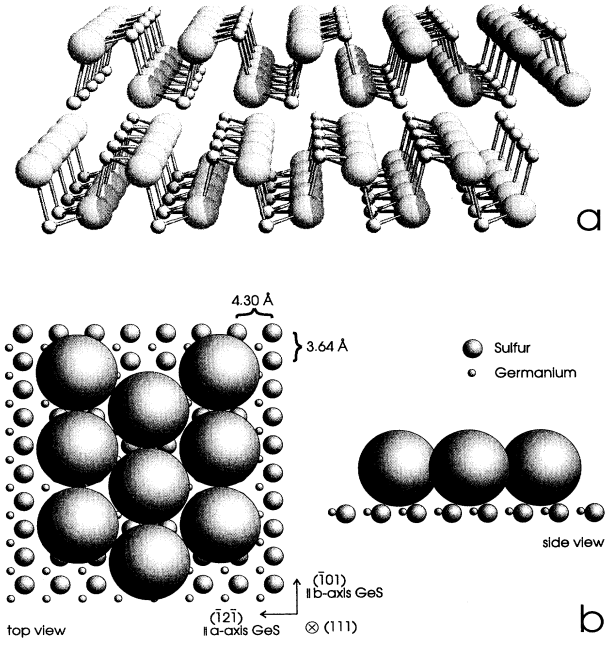

FIG. 1. (a) Structure of the GeS(001) surface. The layered structure of the material is clearly visible. The high surface corrugation due to the grooves along the [010] direction is probably one reason for the comparatively large friction on this material (cf. Table I). (b) Structural model of epitaxial C_{60} monolayers on GeS(001). If the C_{60} molecules fill in every second groove on the GeS surface, an epitaxially oriented monolayer with (111) orientation and very low internal stress can be formed.

cleavage. Highly purified C_{60} material was filled into the graphite crucible of a Knudsen cell, outgassed at 380 °C for several hours and heated to the evaporation temperature of 420 °C 1 h before the evaporation process was started by opening a shutter. During the evaporation process, the substrate temperature was held at 180 °C; the evaporation rate was 0.07 ML/min and the background pressure 2×10^{-9} Pa.

Samples prepared in the way described above have already proven to form epitaxial layers on GeS(001);[18,19] the structural model is shown in Fig. 1(b). Due to the asymmetry of the structure, grooves are formed on the GeS(001) surface parallel to the [010] direction [see Fig. 1(a)]. The period of these grooves (4.30 Å) is nearly half of the distance of two neighbored rows on the (111) surface of a C_{60} crystal (8.67 Å). As every second row is filled with C_{60} molecules [Fig. 1(b)], the C_{60} molecules form an epitaxial (111) layer of a closed-packed structure with the [$\bar{1}$01] direction aligned to the b axis of the GeS substrate. The quality of the C_{60} layers is controlled by LEED after the evaporation process. Due to the crystallinity and the epitaxy of the growing C_{60} islands, a sharp LEED pattern is obtained.[20]

The scanning and friction force microscopy investigation was performed under ambient conditions and at room temperature with a commercially available instrument.[21] Normal and lateral forces were measured simultaneously;[4,5] scan speeds were about 2 μm/s.

Great care was taken in order to obtain not only qualitative, but also reliable quantitative data. A rectangular single-crystalline silicon cantilever[22] was used for all measurements shown below, whose dimensions were accurately determined by means of electron microscopy. Spring constants of 0.045 ± 0.005 N/m in the z direction and 289 ± 60 μN/rad for torsion were calculated according to the formulas given in Ref. 23. The errors of these spring constants are primarily influenced by the errors in the lever thickness t ($t = 1.3 \pm 0.1$ μm) and, for the torsional spring constant, by the error in the tip length l ($l = 13.2 \pm 2.6$ μm).

For the determination of absolute values for normal as well as lateral forces, more possible sources of errors have to be taken into account such as the calibration of the deflection sensor and the varying position of the laser beam on the cantilever. Doing so, a relative error of $\approx$30% for the lateral force data and of $\approx$15% for the normal forces were obtained. These errors, however, are fully systematical. The statistical error of a data point is, as shown below, very small. Therefore, the observed proportionalities should not be affected very much by these quite large errors; the errors are accurately represented by the χ^2 value of the statistical analysis. A detailed analysis of force calibration in lateral force microscopy will be given elsewhere.[24]

The normal forces F_n and the adhesion F_0 were determined through force-versus-distance curves. F_n was set to be zero at the point where the cantilever leaves the surface. A large number of force-versus-distance curves, performed all over the sample, showed no significant variation of the measured adhesion F_0. Only statistical fluctuations were observed. Thus, the zero point of the normal force F_n was taken to be the same for the C_{60} layers and the substrate surface. Recalling that both surfaces interact only by weak van der Waals forces with adsorbed atoms or molecules, this appears to be reasonable.

The lateral forces are averaged over at least 250 individual data points fluctuating by roughly 15% peak to peak, which were accumulated over distances of several hundred nanometers. Thus, the statistical error of an individual data point as displayed in Fig. 4 is very small ($\approx$1%). However, in order to get a feeling for more long-term fluctuations, the lateral forces were determined at the same surface spot twice for each selected normal force value.

III. RESULTS

For the present friction study, a sample with a nominal coverage of 1.2 ML was used. A large-scale topographical image (6.2×6.2 μm^2) is shown in Fig. 2, revealing dendritically shaped C_{60} islands. Due to a nonideal layer-by-layer growth, 30% of the substrate surface was still uncovered, but 40% of the surface was covered by two monolayers and about 4% even by three layers. Details of the growth process are discussed elsewhere.[17,19]

Figure 3 shows topography (a) and friction force maps

FIG. 2. Topographical force micrograph of a sample with a nominal coverage of 1.2 ML of C_{60} molecules, exhibiting dendritically shaped islands of up to 3 ML height. Scan size was 6.2 × 6.2 μm^2.

(b–i) obtained by combined scanning and friction force microscopy. The scanned area was 2×2 μm^2. In the topographical image [Fig. 3(a)], the dendritically shaped C_{60} islands with 1 or 2 ML height are easily observable. The friction force maps presented in Figs. 3(b–i) were

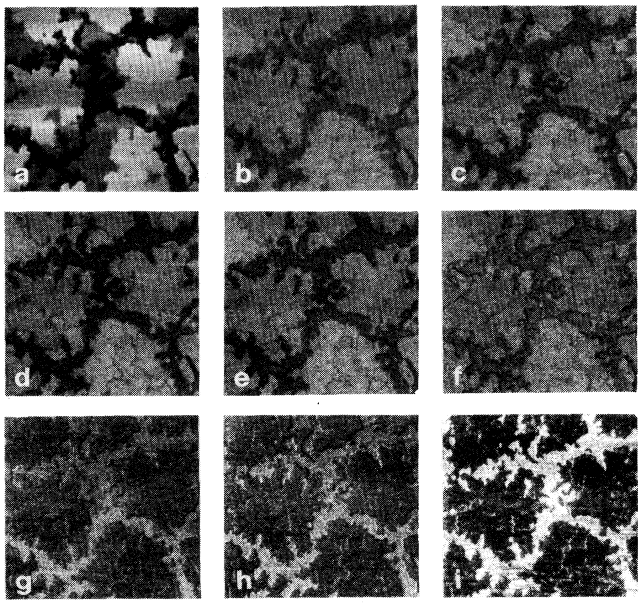

FIG. 3. Topography (a) and friction force maps (b–i) of a spot on the same sample as presented in Fig. 2. The islands are 1–2 ML high (about 1 nm each); scan size was 2 × 2 μm^2. In the friction force maps, dark means low and bright means high frictional force. Normal forces F_n were 1.3 nN for (b), 2.6 nN for (c), 4.5 nN (d), 6.7 nN (e), 10 nN (f), 15 nN (g), 20 nN (h), and 30 nN (i). The contrast flips between 10 nN and 15 nN normal force.

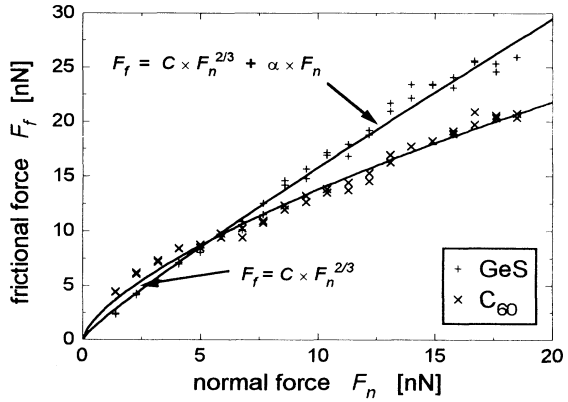

FIG. 4. Plot of F_f as a function of F_n. The data points from the GeS substrate can well be approximated by a curve of roughly linear shape according to Eq. (18) (C = 1.06 $nN^{1/3}$, α = 1.08). For the C_{60} data, the fit according to Eq. (19) ($F_f \propto F_n^{2/3}$) is plotted (C = 2.96 $nN^{1/3}$).

acquired at normal forces F_n ranging from 1.3 to 30 nN on the same spot as shown in Fig. 3(a); dark means low and bright means high frictional force. At low loading forces [Fig. 3(b–e)], the frictional force on the C_{60} islands is obviously higher than on the GeS substrate. With increasing F_n, the contrast gets weaker until it flips above $F_n \approx 10$ nN [Fig. 3(f)]. Further increment of the normal forces [Fig. 3(g–i)] results in significantly lower frictional forces on the C_{60} islands in comparison to the substrate.

This behavior is illustrated by the plot presented in Fig. 4, which shows the frictional force F_f, determined on the first monolayer, as a function of the normal force F_n. The two lines cross at around 7 nN, which corresponds to the flip in the contrast in Fig. 3. The determined normal forces F_n at which the frictional forces on the substrate and on the first C_{60} layer were equal varied between ≈6 and 12 nN in different experiments; the qualitative behavior as discussed below, however, was always the same. Above 20 nN, the C_{60} monolayers start to become modified due to increased tip-sample interaction [see arrow in Fig. 3(i)]. Below this force, no modification of the sample surface could be observed even after extensive scanning

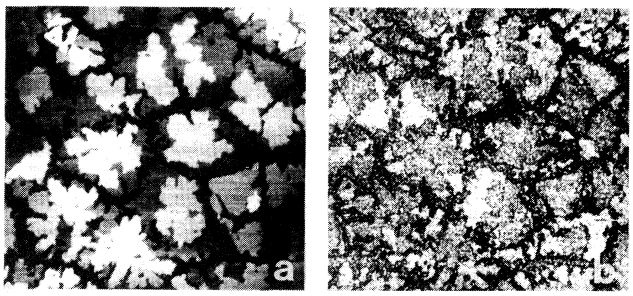

FIG. 5. Topographical force micrograph (a) and simultaneously recorded friction force map (b) of a 4 × 4-μm^2-large area imaged at F_n = 6.7 nN. The second C_{60} monolayer exhibits a numerical value of the frictional force which is just in the middle of the friction on the first monolayer and the friction on the substrate.

(wearless friction). For these data, F_0 was determined to be 6.7 nN.

Taking a closer look at Fig. 3, it can be seen that in some friction force maps acquired at normal forces below the crossing point [Figs. 3(c–f)], the second C_{60} layer is somewhat darker than the first layer, indicating a lower friction on the second than on the first monolayer of C_{60} molecules. This is even better exemplified in Fig. 5, where the topography (a) and the simultaneously recorded friction force map (b) of a 4×4–μm^2-large area are shown. The normal force F_n was 6.7 nN. By means of statistical analysis, it could be shown that, in this image, the frictional force on the second layer is just between the friction on the substrate and the friction on the first monolayer.

IV. DISCUSSION

The theory of friction is governed by Amontons's law, which states that the frictional force F_f is proportional to the *externally applied* loading force F_l (which differs from the normal force F_n acting on the atoms at the contact interface in the case of adhesive junctions, as will be discussed below) for many combinations of materials and independent of the *apparent* area of contact

$$F_f = \mu F_l, \tag{1}$$

where μ denotes the coefficient of friction.

To explain Eq. (1), the structural properties of the contact interface have to be considered. For macroscopic bodies, the *actual* area of contact is limited to discrete spots of the interface due to the roughness of the surface on a microscopic scale. Thus, for a further analysis, it will be convenient to separate the influence of changes in the *actual* area of contact A from the influence of changes in the mean contact pressure p,

$$p = F_l/A, \tag{2}$$

by defining the quantity S,

$$S = F_f/A\ , \tag{3}$$

which represents the frictional force per unit area. Note that A will generally depend on F_l, whereas S can be a function of p. In the present case of wearless shearing of an adhesive junction in the elastic limit, i.e., without any plastic deformation, S is equivalent to the shear strength of the junction according to the Bowden and Tabor model.[7] This model, originally introduced for the adhesive shearing of metallic junctions,[7] has already proven to be a successful concept also for the wearless shearing of other adhesive junctions such as thin organic films or mica on mica.[1,2,25]

First, the nature of the dependence of A on F_l should be discussed. Bowden and Tabor[7] already noticed that Amontons's law holds only when the actual area of contact increases proportionally with the applied load. It can be shown that under certain assumptions about the statistical distribution of asperity heights for rough surfaces of macroscopic bodies or with the consideration of plastic flow, F_f will be proportional to the externally applied load F_l whatever the law of deformation, the shape of the asperities or the nature of the $S(P)$ dependence are.[26,27] However, a load-dependent friction coefficient has been observed on several materials.[1,7,28–31] In most cases, the friction coefficient decreases with increasing load. This is often explained in terms of relationship (3) with a $A \propto F_l^m$ law $(0 < m < 1)$.

In order to get a feeling for the contact mechanics occurring in the case of a small FFM tip sliding over a sample surface, the idealized case of a spherical tip on a perfectly flat surface should be considered. For this situation, Hertz[32,33] showed already more than a hundred years ago that for a nonadhesive junction, the contact area A is given by

$$A_{\mathrm{Hertz}} = \pi a_{\mathrm{Hertz}}^2 = \pi \left(\frac{R}{K} F_l \right)^{2/3}, \tag{4}$$

where a_{Hertz} denotes the radius of the contact area, R the radius of the sphere over the flat, and K the elastic moduli,

$$K = \frac{4}{3} \left(\frac{1-\nu_1^2}{E_1} + \frac{1-\nu_2^2}{E_2} \right)^{-1}$$

(ν_i is Poisson's ratio, E_i is Young's modulus of sphere and flat, respectively; $i = 1,2$). Combining Eqs. (3) and (4) results in the following relationship for the frictional force:

$$F_f = S\pi \left(\frac{R}{K} F_l \right)^{2/3}, \tag{5}$$

which was confirmed in the experiment.[31]

Equation (4) is only valid for nonadhesive junctions. In the present case of a tip over a flat at ambient conditions, attractive forces mainly due to capillary forces occur.[34] Therefore, a modified theory describing the contact mechanics of the tip/sample interface is needed that considers capillary condensation. This is included in the generalized Hertzian theory introduced by Fogden and White[35] (henceforth referred to as FW). It is in principle an extension of the theory of Derjaguin, Muller, and Toporov (Ref. 36, but see also Refs. 37–40), assuming the capillary forces as the only attractive forces acting outside of the contact area.

In this theory, the load-contact area curve is determined by a set of two equations that depend on a fundamental parameter k:

$$k = \frac{3\pi^{1/2}}{2^{3/2}} \frac{K \left(r_k - \frac{1}{2} D_0 \right)^{3/2}}{2\gamma_{\mathrm{LV}} R^{1/2}} \left(1 - \frac{D_0}{2r_k} \right)^{-1}. \tag{6}$$

Here, r_k represents the radius of the meniscus, γ_{LV} the surface tension of the liquid-vapor interface per unit area, and D_0 the separation of the two surfaces. Since these two equations cannot be solved analytically, the FW theory can only be handled numerically with a computer.

Nevertheless, for sufficiently small or large k, analytic approximations can be derived.[35] A small k value describes a system of a soft, large sphere over a soft flat and vapor pressures close to the onset of capillary condensation. In this limit, the additional effect of the attractive capillary forces can be described by the introduction of an *apparent* Hertzian load F^s_{FW}:

$$F^s_{\mathrm{FW}} = F_l + 6\pi R\gamma_{\mathrm{LV}} + \sqrt{12\pi R\gamma_{\mathrm{LV}}F_l + (6\pi R\gamma_{\mathrm{LV}})^2}\ , \tag{7}$$

which is somewhat larger than the *externally* applied load F_l. The mathematics of the FW model in this limit is very similar to the one of the theory of Johnson, Kendall, and Roberts[41] (JKR) developed for junctions that show adhesion due to a finite surface energy of the contact interface. Replacing F_l by F^s_{FW} in Eq. (5), the contact area A^s_{FW} in the small k limit of the FW model can be written as

$$\begin{aligned} A^s_{\mathrm{FW}} &= \pi\left(\frac{R}{K}F^s_{\mathrm{FW}}\right)^{2/3} \\ &= \pi\left(\frac{R}{K}\right)^{2/3} \\ &\quad\times\Big[F_l + 6\pi R\gamma_{\mathrm{LV}} \\ &\quad + \sqrt{12\pi R\gamma_{\mathrm{LV}}F_l + (6\pi R\gamma_{\mathrm{LV}})^2}\Big]^{2/3}. \end{aligned} \tag{8}$$

A consequence of this equation is that at small negative loads ($F_l < 0$ nN), the sphere and the flat still possess a finite contact area (i.e., they still adhere) until the square root becomes zero. At this point, where the "pull-off" force $F^s_{\mathrm{PO}} = -3\pi R\gamma_{\mathrm{LV}}/2$ is reached, the surfaces suddenly disengage.

It has been understood for many years[42,43] that two surfaces in contact can experience an additional load F_0 due to attractive forces. Hence, Amontons's macroscopical law [Eq. (1)] has been modified to

$$F_f = \mu(F_l + F_0) = \mu F_n. \tag{9}$$

$F_n = F_0 + F_l$ denotes the normal component of the forces acting on the sample surface as defined in the experimental part and has to be compensated for by a repulsive force of the sample surface being in contact with the probing tip. The numerical value of F_n is decisive for frictional phenomena or surface modifications. F_0 is equal to the absolute value of the pull-off force F_{PO} and can therefore be determined by force-versus-distance curves.

Hence it follows for the FW theory:

$$F_0 = -F^s_{\mathrm{PO}} = 3\pi R\gamma_{\mathrm{LV}}. \tag{10}$$

This, together with the above definition of F_n, allows us to rewrite Eqs. (7) and (8) in the convenient forms

$$F^s_{\mathrm{FW}} = \left(\sqrt{F_n} + \sqrt{F_0}\right)^2 \tag{11}$$

and

$$A^s_{\mathrm{FW}} = \pi\left(\frac{R}{K}\right)^{2/3}\left(\sqrt{F_n} + \sqrt{F_0}\right)^{4/3}. \tag{12}$$

Combined with Eq. (3), Eq. (12) leads to

$$F_f = S\pi\left(\frac{R}{K}\right)^{2/3}\left(\sqrt{F_n} + \sqrt{F_0}\right)^{4/3}. \tag{13}$$

Note that, in this limit, we get an offset of $F^0_f = S\pi(RF_0/K)^{2/3}$ for $F_n = 0$ nN.

In the limit for large k, corresponding to a small, hard sphere in contact with a hard flat having a well-developed meniscus, it turned out that capillary forces can simply be considered by an apparent Hertzian load F^l_{FW}:

$$F^l_{\mathrm{FW}} = F_l + F_0 = F_n$$

with $F_0 = -F^l_{\mathrm{PO}} = 4\pi R\gamma_{\mathrm{LV}}(1 - D_0/2r_k)$, leading to

$$F_f = S\pi\left(\frac{R}{K}F_n\right)^{2/3}. \tag{14}$$

The contact mechanical models introduced above are derived for static equilibrium conditions. Nevertheless, it was shown recently for the Hertzian and the JKR model that these models also apply for sliding conditions at not too fast sliding velocities.[44] Hence, for a theoretical explanation of the frictional behavior, an interpretation of the measured data in terms of the FW theory seems reasonable. However, before the approximations given above are compared to the experimental data, a closer look should be taken at the parameter k. Assuming a well-developed meniscus with $r_k = 1$ nm or even larger seems reasonable since the measurements were carried out at a relative vapor pressure of approximately 55%, which is well above the critical pressure for meniscus formation. An estimated value of the tip radius is obtained by using $-F_{\mathrm{PO}} = 6.7$ nN $= F_0 = 4\pi R\gamma_{\mathrm{LV}}(1 - D_0/2r_k)$. Setting $D_0 \approx 1$ Å and $\gamma_{\mathrm{LV}} = 72$ mJ/m^2 (surface energy of water) gives $R \approx 7.8$ nm, which is in agreement with the data provided by the manufacturer, who claims tip radii of smaller than 10 nm.[22] With these values and $K \approx 50$ GPa (a typical value for layered materials like GeS in combination with silicon tips; exact values for E_{GeS} and ν_{GeS} are not available), k is calculated to 228. Thus, the large-k model should apply.

In order to make a comparison between the idealized case of tip and sample in Hertzian contact and the results presented above, a model for the dependence of S on the mean pressure p is required. [Note that, in order to consider the contribution of the additional attractive forces caused by the meniscus on the mean pressure, F_l in Eq. (2) has to be replaced by F_n, leading to $p = F_n/A$.] There is no conclusive theory as to how such a dependence should look. However, a popular model that was first proposed by Bridgeman[45] approximates the pressure dependence of S by

$$S = S_0 + \alpha p. \tag{15}$$

The constants S_0 and α determine the frictional properties of the material. In the small-k model, Eq. (15) has to be introduced in Eq. (13), which results in

$$F_f = C\left(\sqrt{F_n} + \sqrt{F_0}\right)^{4/3} + \alpha\left(\sqrt{F_n} + \sqrt{F_0}\right)^2 \quad (16)$$

with

$$C = S_0\pi\left(\frac{R}{K}\right)^{2/3}. \quad (17)$$

For the large-k limit, Eq. (15) has to be combined with Eq. (14), leading to

$$F_f = CF_n^{2/3} + \alpha F_n. \quad (18)$$

Table I shows results of fits of the parameter set given in Fig. 4 according to Eqs. (16) and (18). The results confirm the expectation that the large-k model is probably best suited for the description of the situation. It can be seen that Eq. (16) (small-k model) gives good results, i.e., low values for χ^2, on both materials only for values of $C < 0$ nN$^{1/3}$. The definition of C in Eq. (17), however, obviously only allows values equal or larger than zero. Setting C or, even worse, α to zero results in comparatively high values for χ^2. Hence, the small-k model indeed proves to be not suitable for the situation.

Using Eq. (20), the best fit for the data measured on the GeS substrate is found to be the one with $C = 1.06 \pm 0.22$ nN$^{1/3}$ and $\alpha = 1.08 \pm 0.09$; i.e., both terms contribute considerably to F_f. The solution with $C = 0$ nN$^{1/3}$, however, reveals a value for χ^2 only 50% higher. **Therefore, in spite of being nonlinear, the $F_f(F_n)$ dependence is not very far from a linear model of Amontons's type with $\alpha = 1.53 \pm 0.01$, as also visible from Fig. 4.**

For the data on the C_{60} layers, the situation is different. A straight line through zero is not a possible solution, since this could not explain the observed flip of the contrast in Fig. 3. Furthermore, this fit implies an eight times higher value for χ^2 than the other two fits. These other two fits result in nearly the same curve. In the case where $\alpha \neq 0$, it is very close to zero ($\alpha = 0.03 \pm 0.07$) and can be neglected. Therefore, the dependence of F_f on F_n on the C_{60} monolayers can be excellently approximated by

$$F_f = S_0 A = CF_n^{2/3}, \quad (19)$$

where S_0 has, in contrast to S in Eq. (3), no pressure dependence.

In Fig. 4, the curve according to Eq. (19) is plotted for data obtained on the first C_{60} layer. It can be seen that in the low-load region, the measured data are slightly higher than the calculated curve. From Figs. 3 and 5, however, it was recognized that at these loads the friction on the second C_{60} layer is lower than on the first layer and therefore fits even better the theoretically predicted values. This lower friction on the second layer can probably be explained by a stronger interaction of the C_{60} molecules with the substrate than between individual C_{60} layers, as already found earlier and described in Refs. 20 and 46.

For a comparison with other work, some quantitative values should be calculated. Using $A^l_{\mathrm{FW}} = \pi(RF^l_{\mathrm{FW}}/K)^{2/3} = \pi(RF_n/K)^{2/3}$ (A^l_{FW} is the contact area of the tip and sample calculated according to the FW model in the limit for large k) and again taking $K \approx 50$ GPa and $R \approx 7.8$ nm, A^l_{FW} results in ≈ 0.9 nm^2 for $F_n = 1$ nN and ≈ 4.2 nm^2 for $F_n = 10$ nN. This leads to contact pressures of ≈ 1.1 GPa for $F_n = 1$ nN and ≈ 2.4 GPa for $F_n = 10$ nN. Moreover, with the definition of C according to Eq. (17), $S_0 = CK^{2/3}/\pi R^{2/3}$ can be calculated to 3.3 GPa on the C_{60} layers, using $C = 2.96$ nN$^{1/3}$, and to 1.2 GPa on the GeS substrate, using $C = 1.06$ nN$^{1/3}$. The actual value on the C_{60} layers will probably be somewhat lower if one considers that the value of K accounting for the C_{60} layers is most likely lower than the value of K accounting for the GeS substrate due to an increased softness of the C_{60} molecules. However, even with this uncertainty in the determination of K, it can be stated that S_0 is in the range of gigapascals.

Nevertheless, these values are difficult to compare with values already published, as shown below. The contact pressures, e.g., are slightly higher than the pressures applied in the experiments presented in Ref. 1 and about the same as in the high-pressure regime investigated in Ref. 47 and therefore not very unusual; in these reports, however, the typical values of S_0 are about a factor of 1000 lower. This might be due to the different setups in these experiments (much larger contact areas, other materials, and actual and apparent contact area might differ in these experiments, etc.).

The reason for the different behavior of the frictional force on the two different materials, if interpreted as discussed above, is still unclear since it is not known how S_0 or α are determined by properties like the crystal

TABLE I. Results of the fits for Eqs. (16) and (18) to the data set shown in Fig. 4 (40 data points at 20 different forces). F_0 was 6.7 nN.

Fitted equation	Fit on C_{60} layers			Fit on GeS substrate		
	C (nN$^{1/3}$)	α	χ^2	C (nN$^{1/3}$)	α	χ^2
(16)	-0.95 ± 0.09	0.71 ± 0.03	0.290	-2.91 ± 0.14	1.38 ± 0.04	0.657
(16), $C = 0$ nN$^{1/3}$	0	0.42 ± 0.01	1.062	0	0.50 ± 0.01	7.831
(16), $\alpha = 0$	1.36 ± 0.02	0	4.901	1.63 ± 0.07	0	18.267
(18)	2.89 ± 0.18	0.03 ± 0.07	0.458	1.06 ± 0.22	1.08 ± 0.09	0.672
(18), $C = 0$ nN$^{1/3}$	0	1.25 ± 0.03	3.424	0	1.53 ± 0.01	1.058
(18), $\alpha = 0$	2.96 ± 0.02	0	0.449	3.59 ± 0.06	0	2.964

structure or the atomic species. However, an explanation should be tried in terms of the theory developed by Briscoe and Evans.[1] They derived Eq. (15) using a thermally activated model of Eyring's type, obtaining

$$S_0 = \frac{1}{\Phi}\left\{k_B T \ln\left(\frac{V}{V_0}\right) + Q'\right\} \tag{20}$$

and

$$\alpha = \frac{\Omega}{\Phi}, \tag{21}$$

where k_B is Boltzmann's constant, T the temperature, V the sliding velocity, V_0 a proportional constant determined by the frequency of the thermally activated lattice vibration and the lattice parameters, Q' is the height of the potential barrier between two minima of the surface potential without any applied force, and Ω and Φ are constants, formally having the units of volumes, but describing the change of the potential barrier under the influence of a normal (Ω) or lateral (Φ) force.

Unfortunately, the physical meaning of some of the constants is not clear. V_0 should be determined, as mentioned above, by the frequency of the thermally activated lattice vibration and the lattice parameters, but an exact value cannot be given. The parameters Ω and Φ arise automatically from the theory to make the activation terms dimensionally correct, but are difficult to interpret. The stress activation volume Φ is generally interpreted as the size segment that moves in the unit shear process. In the study of Briscoe and Evans, which was performed using an SFA, this volume had a size of several molecules (1.6–6.6 nm^3) in the case of thin films of stearic or behenic acid deposited on mica. The pressure activation volume Ω is associated with the local increase in volume at a strategic site in the lattice, which is necessary to permit the molecular motion to occur. Briscoe and Evans found, again for stearic and behenic acid, values for Ω of about 0.1 nm^2, which is approximately the volume of an ethyl group of the used molecules. Nevertheless, these interpretations are very uncertain and should be used with extreme care. Furthermore, the values of Ω and Φ might be temperature, scan rate, and pressure dependent and might significantly differ at different experimental conditions.

On the GeS substrate, $S_0 = 1.2$ GPa and $\alpha = 1.08$ was found. This means that the volumes Ω and Φ have nearly the same size, differing from what was found, e.g., in the study of Briscoe and Evans.[1] There, the value of Ω is much lower than the value of Φ, resulting in values for α between 0.01 and 0.3. On the other hand, a low value for Φ explains well the comparably high value for S_0, if values in the same order of magnitude for Q' and $\ln(V/V_0)$ as in Ref. 1 are assumed. This might indicate that only very few atoms are involved in the slipping process at the atomic scale, probably due to the groovelike surface structure or the small contact area.

For the results on the C_{60} layers, the high value of $S_0 \approx 3.3$ GPa can be explained by a higher value for the potential barrier Q' due to the large corrugation of the $C_{60}(111)$ surface, but also by a low value for Φ again. Thus, low values for Φ might be an intrinsic property of FFM since, there, only few atoms are involved in the slipping process. On the other hand, to obtain $\alpha \approx 0$, a low value for Ω is needed. Recalling that Ω is a measure for the dependence of the potential barrier height on the external pressure, this implies that the friction on the C_{60} molecules should not depend on the pressure at the contact interface, in agreement with the experimental findings.

The above interpretation is based on the assumptions that (1) the tip/sample junction represents an ideal Hertzian contact and (2) $S(P)$ can be described by $S(P) = S_0 + \alpha P$. However, this might not necessarily be true. Furthermore, it is not easily understandable why the potential barrier on the GeS substrate should be pressure dependent and the potential barrier on the C_{60} monolayers is not. Therefore, the above model should be generalized introducing a non-Hertzian tip/sample contact. Such a non-Hertzian tip/sample contact is likely to occur in the case of FFM tips, which cannot be expected to be perfectly round shaped.

Greenwood[26,27] showed, as already mentioned above, that for arbitrarily shaped surfaces, the actual contact area will be proportional to the load. In the Hertzian case, we know that the contact area is proportional to $F_n^{2/3}$. Pyramidal-shaped or conical tips exhibit dependencies proprotional to $F_n^{1/2}$. Therefore, at least relatively small force variations, the contact-area–load dependence might be well approximated by a more general $A \sim F_n^m$ law with $0 < m < 1$:

$$A = C' F_n^m. \tag{22}$$

Thereby, C' is a constant in units adequate to m. This results in the following equation for the frictional force

$$F_f = C'' F_n^m + \alpha F_n \tag{23}$$

with $C'' = S_0 C'$. Additionally, it has to be considered that the area-load dependence will most probably differ for the tip on the GeS substrate in comparison with the tip on the C_{60} layers due to the much larger corrugation of the C_{60} layers.

With this additional fit parameter m, there are several possibilities to choose C'', α, and m in order to obtain good agreement with the experimental data. However, it is instructive to discuss a special case. Suppose that in the low-load region investigated in this study (i.e., the regime with wearless friction and without the occurrence of plastic deformation), $S = S_0$ is always constant, i.e., $\alpha = 0$. This would rule out the need to explain why the potential barrier on the GeS substrate is pressure dependent and on the C_{60} it is not.

Fitting this model to the data obtained on the GeS substrate (Fig. 4) results in $m = 0.891 \pm 0.020$ and a low χ^2 of 0.637 (cf. Table I). Following the same procedure for the data on the C_{60} layers leads to $m = 0.666 \pm 0.017$ ($\chi^2 = 0.460$), indicating a perfect Hertzian contact. A control measurement, performed with the same tip, reproduced the value on the GeS substrate within 2% ($m = 0.910 \pm 0.010$) and the one on the C_{60} layers within

better than 0.2% ($m = 0.665 \pm 0.012$). A reproducibility of m within 2% from one measurement to another is already very good for FFM experiments performed in air, showing that the tip has nearly not changed. Typical reproducibilities are within $\pm 10\%$.[48] A reproducibility of better than 0.2%, however, is exceptional. Moreover, the fact that on the C_{60} layers a value for m of exactly 2/3 was repetitively obtained is remarkable; for other samples, m normally varies from below 0.5 up to more than 1 for the kind of tip chosen in our experiments.

V. CONCLUSION

In this paper, wearless friction of highly oriented monolayers of C_{60} molecules epitaxially grown on GeS(001) substrates and of the GeS substrate itself has been investigated using friction force microscopy. On the GeS substrate, the frictional force was found to be proportional to the loading force in first approximation ($m \approx 0.9$). For the C_{60} layers, the frictional force can be interpreted as being proportional to the contact area under Hertzian contact without any further contact pressure dependence. This different frictional behavior results in a flip of the contrast in spatially resolved friction force maps as a function of the applied loading force. Additionally, the frictional force on the second C_{60} monolayer was determined to be slightly lower than the frictional force on the first layer at low normal forces.

A model was proposed to explain the different frictional behavior on the two materials. In a first step, a perfect Hertzian contact and a dependence of S on p according to $S = S_0 + \alpha p$ was postulated. Later, the model was extended introducing a more general contact-area–load dependence according to $A \sim F_n^m$, which differs on the C_{60} layers compared with the GeS substrate. It was shown that already for a simple model with $S = S_0$, the observed frictional behavior can be well described.

Future experiments as well as theoretical considerations should aim at clarifying the following questions.

(i) What is the influence of the tip shape on the measured friction? For a correct interpretation of FFM measurements and to really obtain information about the shear strength S, it might be necessary to control the tip shape down to the atomic scale in order to know the exact contact-area–load dependence.

(ii) From SFA studies, it is well known that the presence of surface adsorbates (e.g., water molecules when measured under ambient conditions) has a strong influence on the frictional behavior.[2] Similar observations were reported for FFM investigations.[49] What is the influence of such adsorbates in the case of small contact areas of only nm^2 size, and is it comparable to the case of large contact areas? What happens on the molecular scale?

(iii) It was found that the frictional force on the second C_{60} layer was lower than on the first layer for some values of the normal force, probably due to the stronger interaction of the C_{60} molecules with the substrate than between individual layers. What is the mechanism of this reduction in friction? Is it due to a slower rotation of the individual molecules in the first layer? What is the influence of the rotation of the C_{60} molecules on the friction?

(iv) In this paper, different contact mechanical models have been discussed for the interpretation of the data. Evidence for a validity of these models in the case of very small spheres with a diameter of only some atoms under nonsliding conditions comes from molecular dynamics simulations.[50] However, these models, derived for equilibrium conditions using classical elasticity theory, might not necessarily work in the case of sliding spheres exhibiting very small radii.

ACKNOWLEDGMENTS

We are indebted to O. Wolter for helpful support of this work. Additionally, we thank H. Bluhm, P. Köster, and M. Löhndorf for useful discussions. Financial support of the Deutsche Forschungsgemeinschaft (Grant No. WI 1227/1-2) is gratefully acknowledged.

[1] B. J. Briscoe and D. C. B. Evans, Proc. R. Soc. London Ser. A **380**, 389 (1982).
[2] A. M. Homola, J. N. Israelachvili, P. M. McGuiggan, and M. L. Gee, Wear **136**, 65 (1990).
[3] C. M. Mate, G. M. McClelland, R. Erlandsson, and S. Chiang, Phys. Rev. Lett. **59**, 1942 (1987).
[4] O. Marti, J. Colchero, and J. Mlynek, Nanotechnol. **1**, 141 (1990).
[5] G. Meyer and N. M. Amer, Appl. Phys. Lett. **57**, 2089 (1990).
[6] G. Binnig, C. F. Quate, and C. Gerber, Phys. Rev. Lett. **56**, 930 (1986).
[7] F. P. Bowden and D. Tabor, *The Friction and Lubrication of Solids, Part 2* (Clarendon, Oxford, 1964).
[8] H. W. Kroto, J. R. Heath, S. C. O'Brian, R. F. Curl, and R. E. Smalley, Nature **318**, 162 (1985).
[9] C. S. Yannoni, R. D. Johnson, G. Meijer, D. S. Bethune, and J. R. Salem, J. Phys. Chem. **95**, 9 (1991).
[10] P. J. Blau and C. E. Haberlin, Thin Solid Films **219**, 129 (1992).
[11] B. Bhudhan, B. K. Gupta, G. W. Van Cleef, C. Capp, and J. V. Coe, Appl. Phys. Lett. **62**, 3253 (1993).
[12] J. Ruan and B. Bhushan, J. Mater. Res. **8**, 3019 (1993).
[13] T. Thundat, R. J. Warmack, D. Ding, and R. N. Compton, Appl. Phys. Lett. **63**, 891 (1993).
[14] R. Lüthi, H. Haefke, E. Meyer, L. Howald, H.-P. Lang, G. Gerth, and H.-J. Güntherodt, Z. Phys. B **95**, 1 (1994).
[15] R. Lüthi, E. Meyer, H. Haefke, L. Howald, W. Gutmannsbauer, and H.-J. Güntherodt, Science **266**, 1979 (1994).
[16] T. Grandke and L. Ley, Phys. Rev. B **16**, 832 (1977).

[17] W. Allers, U. D. Schwarz, G. Gensterblum, and R. Wiesendanger, Appl. Phys. A **59**, 11 (1994).
[18] G. Gensterblum, K. Hevesi, B.-Y. Han, L.-M. Yu, J.-J. Pireaux, P. A. Thiry, R. Caudano, A.-A. Lucas, D. Bernaerts, S. Amelinckx, G. Van Tendeloo, G. Bendele, T. Buslaps, R. L. Johnson, M. Foss, R. Feidenhans'l, and G. Le Lay, Phys. Rev. B **50**, 11 981 (1994).
[19] U. D. Schwarz, W. Allers, G. Gensterblum, J.-J. Pireaux, and R. Wiesendanger, Phys. Rev. B **52**, 5967 (1995).
[20] J.-M. Themlin, S. Bouzidi, F. Coletti, J.-M. Debever, G. Gensterblum, L.-M. Yu, J.-J. Pireaux, and P. A. Thiry, Phys. Rev. B **46**, 15 602 (1992).
[21] Nanoscope III, Digital Instruments, Santa Barbara, CA.
[22] Nanosensors, Aidlingen, Germany.
[23] L. D. Landau and E. M. Lifschitz, *Lehrbuch der Theoretischen Physik, Vol. VII: Elastizitätstheorie*, 6th ed. (Akademie Verlag, Berlin, 1989).
[24] P. Köster, U. D. Schwarz, and R. Wiesendanger (unpublished).
[25] B. J. Briscoe and D. Tabor, J. Adhesion **9**, 145 (1978).
[26] J. A. Greenwood, Transactions of the American Society of Mechanical Engineers [J. Lubrication Technol. **1**, 81 (1967)].
[27] J. A. Greenwood, in *Fundamentals of Friction: Microscopic and Macroscopic Processes*, edited by I. L. Singer and H. M. Pollock (Kluwer Academic Publishers, Dordrecht, 1992), pp. 57–76.
[28] R. C. Bowers, J. Appl. Phys. **42**, 4961 (1971).
[29] K. Miyoshi, Surf. Coatings Technol. **36**, 487 (1988).
[30] R. C. Bowers and W. A. Zisman, J. Appl. Phys. **39**, 5385 (1968).
[31] I. L. Singer, R. N. Boister, J. Wegand, and S. Fayeulle, Appl. Phys. Lett. **57**, 995 (1990).
[32] H. Hertz, J. Reine Angew. Math. **92**, 156 (1881).
[33] For a good review over contact models, see K. L. Johnson, *Contact Mechanics* (Cambridge University Press, Cambridge, 1985).
[34] E. Meyer and H. Heinzelmann, in *Scanning Tunneling Microscopy II*, edited by R. Wiesendanger and H.-J. Güntherodt, Springer Series in Surface Sciences Vol. 28 (Springer-Verlag, Berlin, 1992).
[35] A. Fogden and L. R. White, J. Colloid Interface Sci. **138**, 414 (1990).
[36] B. V. Derjaguin, V. M. Muller, and Y. P. Toporov, J. Colloid Interface Sci. **53**, 314 (1975).
[37] B. D. Hughes and L. R. White, Q. J. Mech. Appl. Math. **33**, 445 (1979).
[38] V. M. Muller, V. S. Yuschenko, and B. V. Derjaguin, J. Colloid Interface Sci. **77**, 91 (1980).
[39] V. M. Muller, V. S. Yuschenko, and B. V. Derjaguin, J. Colloid Interface Sci. **92**, 92 (1983).
[40] A. Burgess, B. D. Hughes, and L. R. White (unpublished).
[41] K. L. Johnson, K. Kendall, and A. D. Roberts, Proc. R. Soc. London Ser. A **324**, 301 (1971).
[42] B. V. Derjaguin, Phis. Khim. **5**, 1163 (1934).
[43] D. Dowson, *History of Tribology* (Longman, London, 1979).
[44] A. M. Homola, J. N. Israelachvili, M. L. Gee, and P. M. McGuiggan, Transactions of the American Society of Mechanical Engineers [J. Tribology **111**, 675 (1989)].
[45] P. W. Bridgeman, Proc. Am. Acad. Arts Sci. **71**, 387 (1936).
[46] G. Gensterblum, L.-M. Yu, J.-J. Pireaux, P. A. Thiry, R. Caudano, J.-M. Themlin, S. Bouzidi, F. Coletti, and J.-M. Debever, Appl. Phys. A **56**, 175 (1993).
[47] J.-M. Georges and D. Mazuyer, J. Phys. Condens. Matter **3**, 9545 (1991).
[48] J. Hu, X.-D. Xiao, D. F. Ogletree, and M. Salmeron, Surf. Sci. **327**, 358 (1995).
[49] M. Binggeli and C. M. Mate, Appl. Phys. Lett. **65**, 415 (1994).
[50] J. Belak and I. F. Stowers, in *Fundamentals of Friction: Microscopic and Macroscopic Processes* (Ref. 27), pp. 511–520.

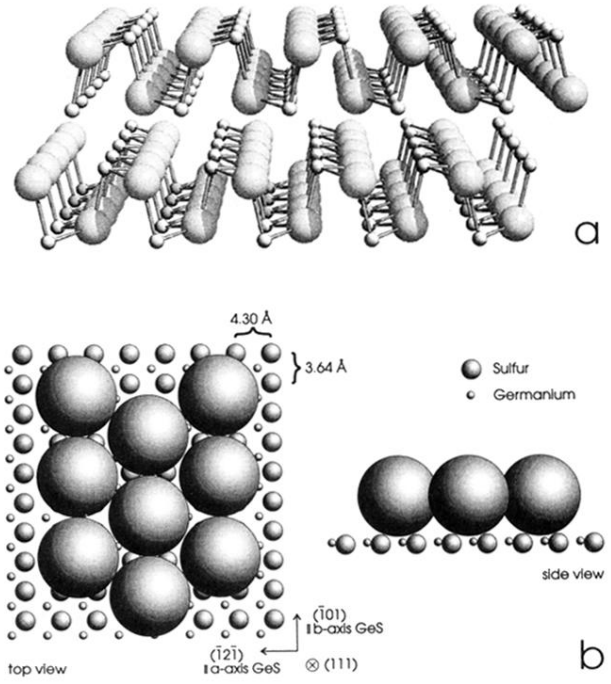

FIG. 1. (a) Structure of the GeS(001) surface. The layered structure of the material is clearly visible. The high surface corrugation due to the grooves along the [010] direction is probably one reason for the comparatively large friction on this material (cf. Table I). (b) Structural model of epitaxial C_{60} monolayers on GeS(001). If the C_{60} molecules fill in every second groove on the GeS surface, an epitaxially oriented monolayer with (111) orientation and very low internal stress can be formed.

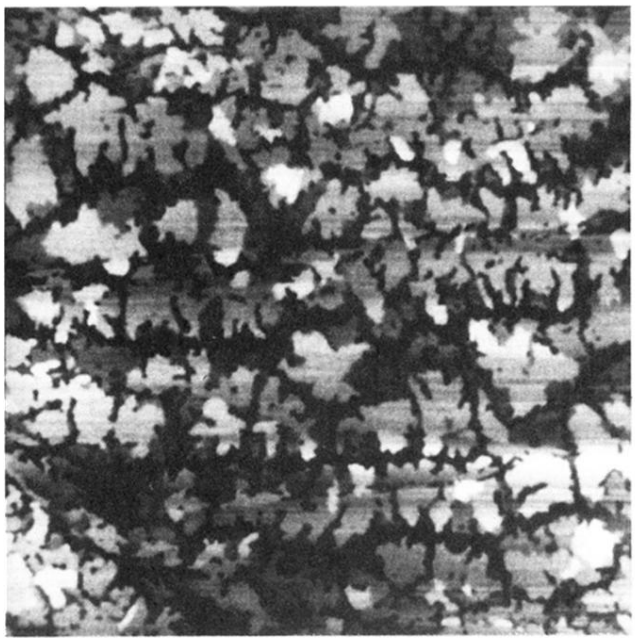

FIG. 2. Topographical force micrograph of a sample with a nominal coverage of 1.2 ML of C_{60} molecules, exhibiting dendritically shaped islands of up to 3 ML height. Scan size was 6.2 $\times$ 6.2 μm^2.

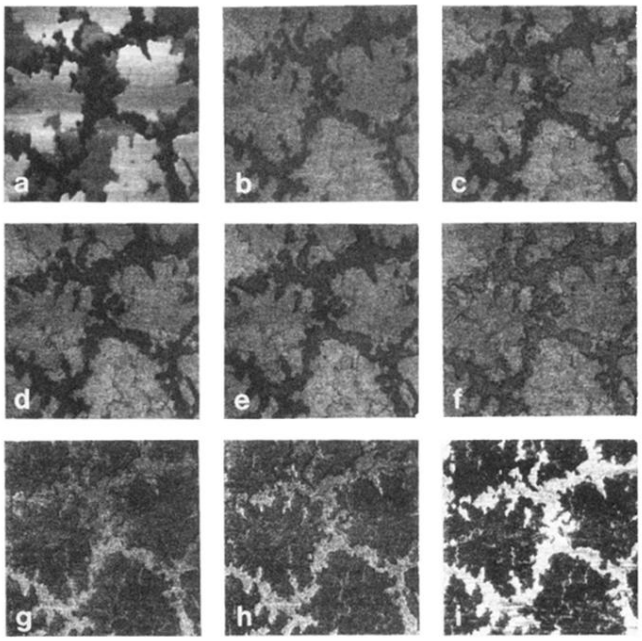

FIG. 3. Topography (a) and friction force maps (b–i) of a spot on the same sample as presented in Fig. 2. The islands are 1–2 ML high (about 1 nm each); scan size was $2 \times 2\ \mu m^2$. In the friction force maps, dark means low and bright means high frictional force. Normal forces F_n were 1.3 nN for (b), 2.6 nN for (c), 4.5 nN (d), 6.7 nN (e), 10 nN (f), 15 nN (g), 20 nN (h), and 30 nN (i). The contrast flips between 10 nN and 15 nN normal force.

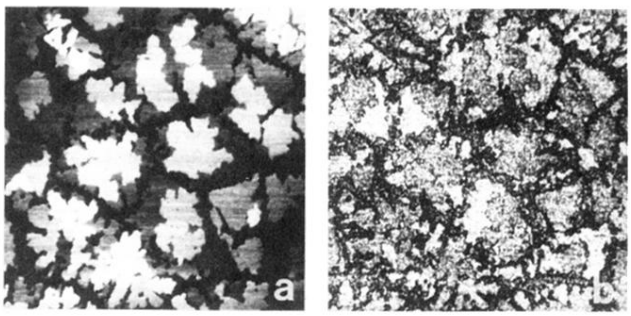

FIG. 5. Topographical force micrograph (a) and simultaneously recorded friction force map (b) of a 4×4-μm^2-large area imaged at $F_n = 6.7$ nN. The second C_{60} monolayer exhibits a numerical value of the frictional force which is just in the middle of the friction on the first monolayer and the friction on the substrate.